

Flow and the equation of state of nuclear matter

P. Danielewicz^a *

^a National Superconducting Cyclotron Laboratory and
Department of Physics and Astronomy, Michigan State University,
East Lansing, Michigan 48824, USA

The status of flow in heavy-ion collisions and of inference of hadronic-matter properties is reviewed.

1. INTRODUCTION

Collective flow is a motion characterized by space-momentum correlations of dynamic origin. It is of interest in collisions because it may tell us about pressures generating that motion and about the equation of state (EOS) and other properties of the strongly-interacting matter. The flows that have been identified thus far are radial, sideward, and elliptic.

The role played by the pressure p in the dynamics may be inferred by examining the relativistic Euler equation in the frame of the matter, defined by vanishing collective velocity $v = 0$:

$$(e + p) \frac{\partial}{\partial t} \vec{v} = -\vec{\nabla} p. \quad (1)$$

Here e is energy density. This equation is an analog of the Newton equation and enthalpy $w = e + p$ plays the role of mass. Pressure plays the role of potential for the collective motion.

Recent interest in the flows and EOS is due to the possibility of identifying the phase transition to quark-gluon plasma. Figure 1 shows a schematic diagram of temperatures T and baryon chemical potentials μ explored in central heavy-ion reactions with the indicated possible crossings of the transition at different accelerators.

In terms of baryon density ρ , the pressure is:

$$p = \rho^2 \left. \frac{\partial(e/\rho)}{\partial \rho} \right|_{s/\rho}, \quad (2)$$

where s is the entropy density. Expected changes in the energy per baryon e/ρ , if there were a phase transition at $T = 0$, are qualitatively indicated in Fig. 2. The arrow in the figure represents the Maxwell construction.

Within and above any first-order phase-transition, or a transitional region, a physical system exhibits a softening, i.e. the ratios p/e and p/w drop. This is due to the fact that

*e-mail: danielewicz@nscl.msu.edu

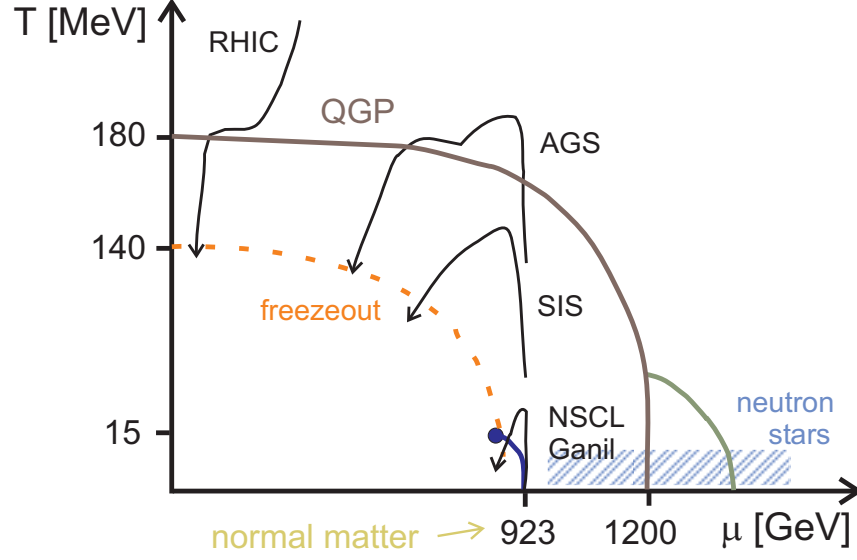


Figure 1. Temperatures T and baryon chemical potentials μ explored in central heavy-ion reactions.

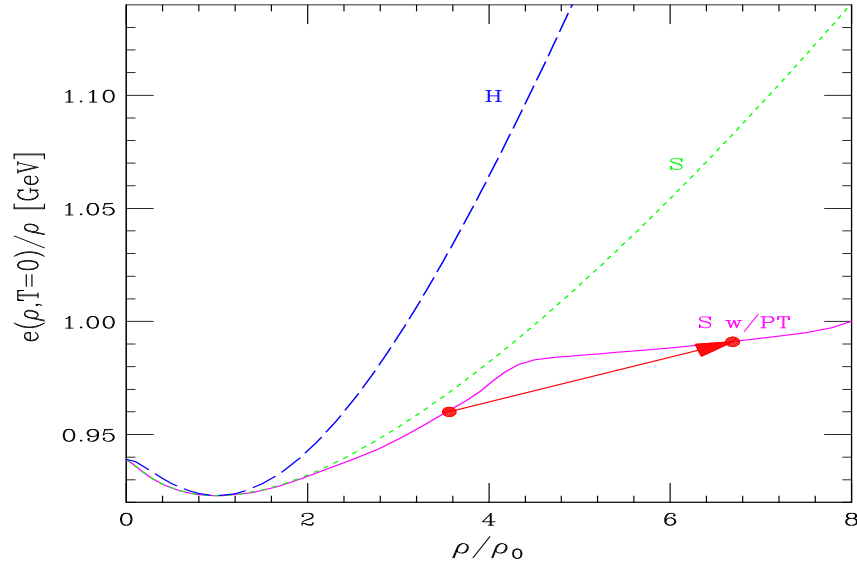


Figure 2. Energy per baryon e/ρ as a function of baryon density ρ , in units of normal density ρ_0 , for a soft EOS (S), hard EOS (H), and a soft EOS with a high-density phase transition (S w/PT).

the pressure p changes *continuously* across the transition, while e jumps together with entropy s and density ρ . For example, in the baryonless matter we have:

$$dp = s dT, \quad de = T ds. \quad (3)$$

With an increase in temperature across a transition, the entropy jumps and so does the energy. However, for the pressure only the derivative changes. Analogous changes across a $T = 0$ transition are deduced in Fig. 2. Following (1), the signature of a phase transition should be a slowed down pace of the development of the nuclear collective motion within and above the phase transition.

Equilibrium, to which EOS and our considerations so far refer to, is never precisely reached in reactions. This creates both difficulties and opportunities. On one hand, extrapolations must be done to the equilibrium limit. On the other hand, the flow may be exploited in exploring the transport properties of hadronic matter, related to in-medium cross sections. The flow may be studied to a variable degree of detail. A study of nucleon flow as a function of transverse momentum, for example, may reveal the dependence of the mean field (MF) felt by nucleons on momentum [1].

We now turn to the different types of flow.

2. RADIAL EXPANSION

The collective radial expansion is often assessed by looking for deviations of momentum distributions, especially transverse, from thermal. The momentum distributions are commonly described in terms of the simple Siemens-Rasmussen [2] formula, or its derivatives,

$$\epsilon \frac{dN}{d\mathbf{p}} \propto e^{-\gamma\epsilon/T} \left\{ \frac{1}{pv} (\gamma\epsilon + T) \sinh \frac{\gamma pv}{T} - \cosh \frac{\gamma pv}{T} \right\}. \quad (4)$$

A safer assessment of the radial flow is by comparing spectra, or average energies, of particles with different mass. The higher the mass, the stronger is the effect of collective expansion and flatter the distribution (more spread-out by the collective velocity), and higher the average energy. Transverse distributions flattening with the particle mass have been seen in central collisions of heavy nuclei at beam energies ranging from below 100 MeV/nucleon to above 100 GeV/nucleon, cf. Fig. 3. The larger-mass distributions are sharper in the lighter than in the heavier system, at the high energy, indicating a weaker collective expansion in the lighter system.

Figure 4 displays excitation function of transverse temperature and of velocity in heaviest systems. The velocity saturates at AGS energies, possibly due to meson production and progressing transparency.

Of interest is the possible use of the radial expansion in the determination of EOS. It must be remembered that the separation into the collective and thermal energies occurs at freeze-out, when collisions become infrequent. Let us consider first the situation at low energies. If the EOS is soft and pressure low, the expansion is slower than for a stiff EOS, but then one just needs to wait longer for same observable values to emerge at freeze-out. To tell the difference, one needs some timing device. As such devices might serve the persistence of longitudinal motion at high energies or the early strange particle emission. Till now though, their exploitation in the EOS determination has been limited [5].

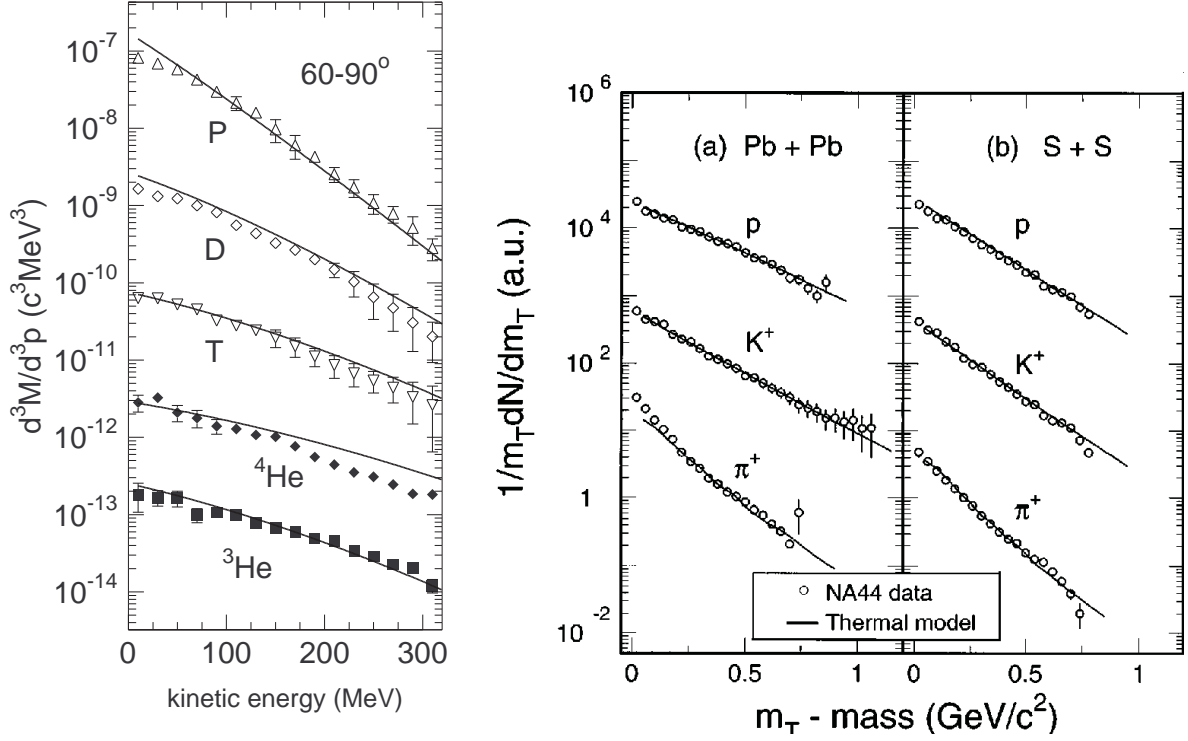


Figure 3. Transverse momentum distributions in central collisions at 250 MeV/nucleon (left) and at 158 GeV/nucleon (right) from the measurements of the FOPI [3] and of the NA44 [4] Collaborations, respectively.

3. SIDEWARD FLOW

Sideward flow is a deflection of forwards and backwards moving particles, away from the beam axis, within the reaction plane. The situation in reactions is schematically illustrated in Fig. 5. For the compressed and excited matter in a central region it is easier to get out to the vacuum on one side of the beam axis than on the other. Eagerness to get out will be enhanced by high generated pressure but also by the momentum dependence of MFs before the equilibration takes place. The ability to get out depends on the inter-particle cross sections.

The sideward flow is often represented in terms of the mean in-plane component of transverse momentum at a given rapidity, $\langle p^x(y) \rangle$, and additionally quantified in terms of the derivative at the midrapidity, see Fig. 6:

$$F_y = \frac{d\langle p^x \rangle}{dy} \quad \text{or} \quad F = \frac{d\langle p^x \rangle}{d(y/y_B)}. \quad (5)$$

The normalization of the rapidity to the beam in the derivative enhances, somewhat artificially, the strength of dynamic effects at high energies relative to low.

In transport models, it is directly observed that the production of sideward flow is shifted towards the high density phase [7] as compared to the radial flow [8]. The sideward

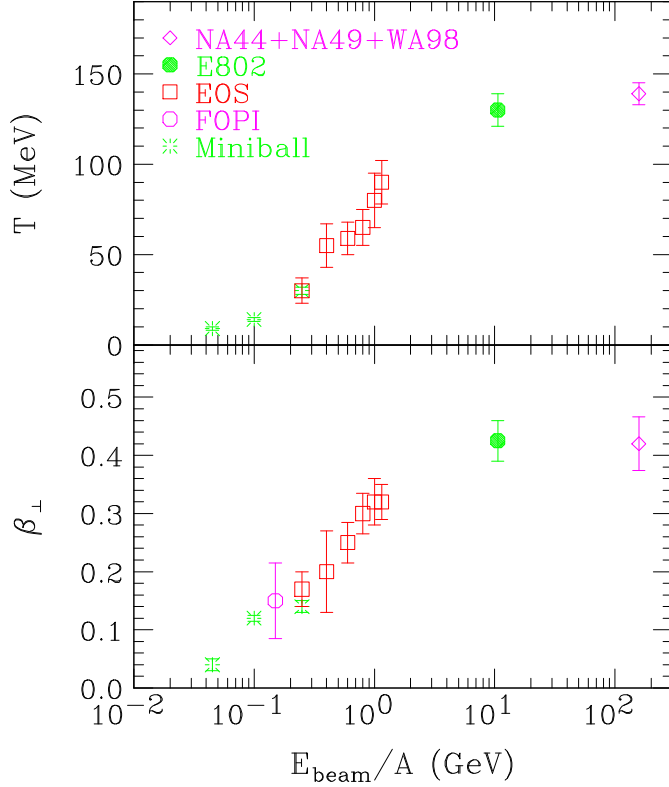


Figure 4. Excitation functions of transverse temperature (upper panel) and transverse collective velocity (lower panel) at midrapidity in heavy systems.

flow thus has more potential in the EOS determination than the radial flow. The flow excitation function is represented in Fig. 7 and the flow is seen to be maximal between 0.1 and 10 GeV/nucleon.

4. SECOND-ORDER OR ELLIPTIC FLOW

The elliptic flow is typically studied at midrapidity and quantified in terms of v_2 :

$$v_2 = \langle \cos 2\phi \rangle \quad (v_n = \langle \cos n\phi \rangle), \quad (6)$$

where ϕ is the azimuthal angle relative to the reaction plane. The second-order flow may offer a better chance for the EOS determination than the first-order sideward flow, because it involves less of the uncertainties in the opposing streams of matter moving past each other. Typical azimuthal patterns at midrapidity may be seen in Fig. 8.

At AGS energies the elliptic flow results from a competition between the early squeeze-out when compressed matter tries to move out in the direction perpendicular to the reaction plane and the late-stage in-plane emission associated with the shape of the participant zone [10], cf. Fig. 9. The squeeze-out contribution to the elliptic flow depends, generally, on the pressure p built-up early on, compared to the energy density e , see (1), and on the passage time for the spectators. When the heated matter is exposed to the

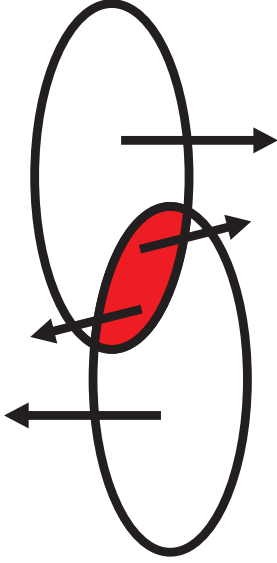


Figure 5. In-plane particle deflection.

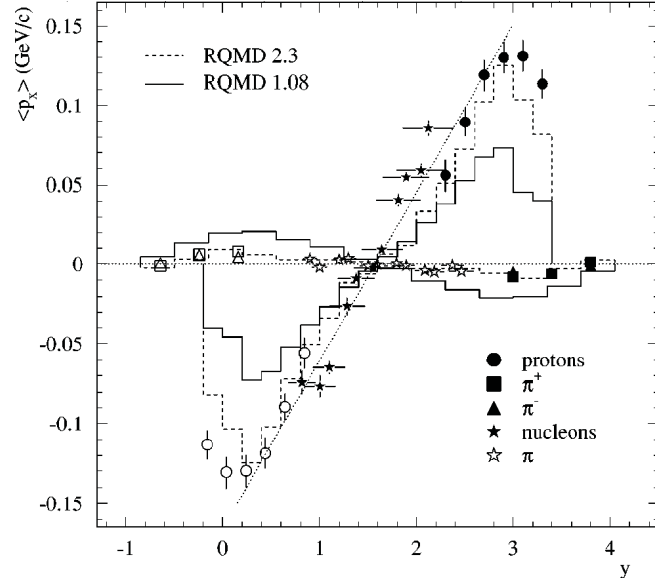


Figure 6. Average in-plane transverse momentum component as a function of rapidity in central Au + Au collisions at 10 GeV/nucleon [6].

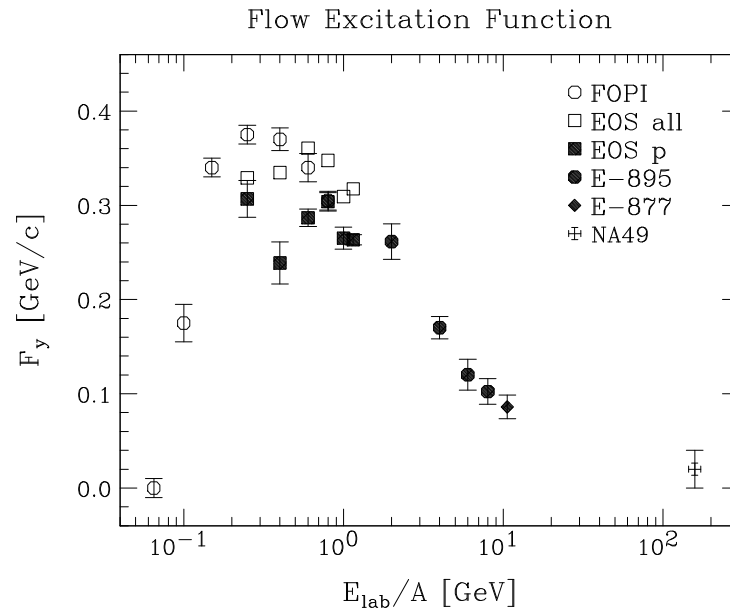


Figure 7. Excitation function of sideward flow in central collisions of heavy nuclei.

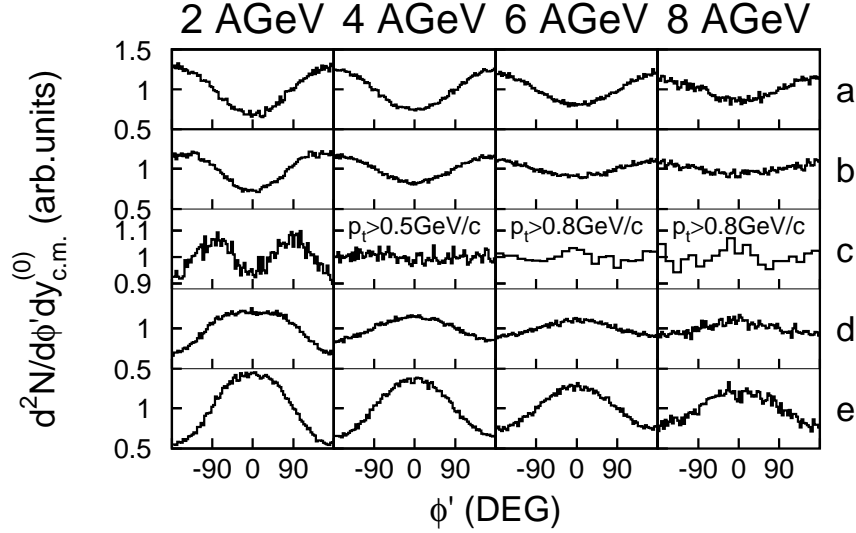


Figure 8. Azimuthal distributions, with respect to the reconstructed reaction plane, of protons emitted from semicentral Au + Au collisions [9] in the rapidity intervals of $-0.7 < y/y_{Beam} < -0.5$ (a), $-0.5 < y/y_{Beam} < -0.3$ (b), $-0.1 < y/y_{Beam} < 0.1$ (c), $0.3 < y/y_{Beam} < 0.5$ (d), and $0.5 < y/y_{Beam} < 0.7$ (e).

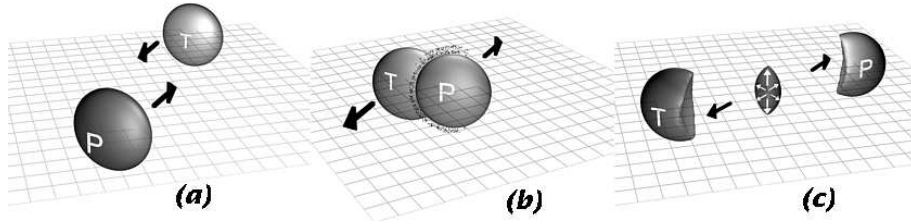


Figure 9. Collision of two Au nuclei at relativistic energies. Time shots are shown for an instant before the collision (a), early in the collision (b), and late in the collision (c).

vacuum in the transverse direction, a rarefaction wave moves in putting the matter into motion. The time for developing the expansion is then R/c_s , where R is the nuclear radius and $c_s = \sqrt{(\partial p / \partial e)_{s/\rho}}$ is the speed of sound. The passage time for spectators, on the other hand, is of the order of $2R/(\gamma_0 v_0)$, where v_0 is the spectator c.m. velocity. The squeeze-out contribution to the elliptic flow should then reflect the time ratio

$$\frac{c_s}{\gamma_0 v_0}. \quad (7)$$

The result (7) gives hope that significant changes in the dependence of pressure on energy density, such as associated with a phase transition,² might be revealed in the

²Discussion of the physics of refraction into mixed phase or across the transition may be found in [11].

variation of the elliptic flow. Overall, the squeeze-out contribution should decrease as a function of energy with the flow becoming positive, $v_2 > 0$. The elliptic-flow excitation function is displayed in Fig. 10. It is seen that, indeed, while dominated by squeeze-out

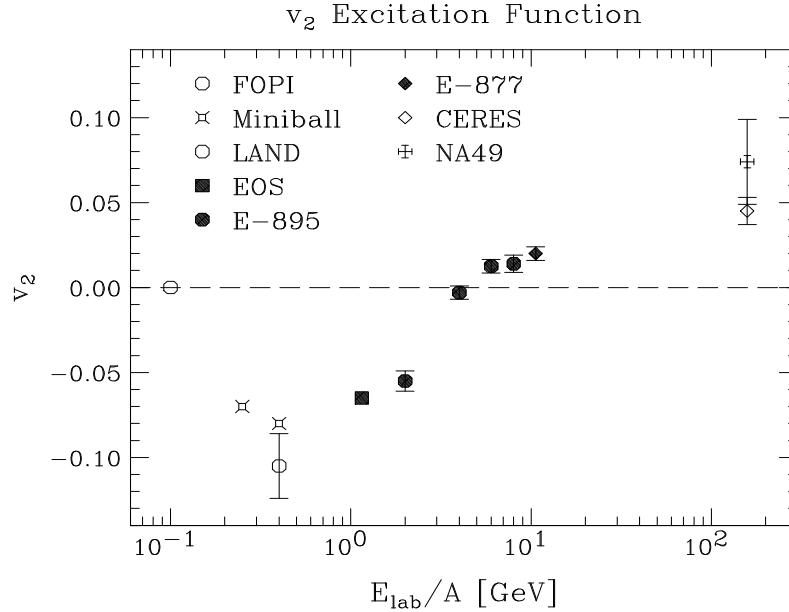


Figure 10. Elliptic-flow excitation function.

at moderate energies, the elliptic flow becomes positive at high energies. Whether or not any changes in v_2 with energy might be associated with any phase transition requires comparisons to transport-model calculations to assess the magnitude of such possible changes. It should be noted, due to the expansion of elliptically shaped participant zone exposed from all sides to the vacuum, Fig. 9(c), the in-plane elliptic flow is expected to be present at RHIC energies, see Fig. 11.

To assess the practical quantitative level of sensitivity of flow observables to EOS and to other characteristics of the medium, we now turn to transport model simulations.

5. TRANSPORT-MODEL COMPARISONS

We shall examine results of a model formulated within relativistic Landau theory, with nucleon, pion, delta and N^* degrees of freedom. The Wigner distribution functions f of those particles follow a set of Boltzmann equations, of the same general for relativistically, as nonrelativistically,

$$\frac{\partial f}{\partial t} + \frac{\partial \epsilon_{\mathbf{p}}}{\partial \mathbf{p}} \frac{\partial f}{\partial \mathbf{r}} - \frac{\partial \epsilon_{\mathbf{p}}}{\partial \mathbf{r}} \frac{\partial f}{\partial \mathbf{p}} = I. \quad (8)$$

The single particle energies ϵ are functional derivatives of an energy functional specified in terms of the Wigner functions f . Specific parametrizations of the functional lead to

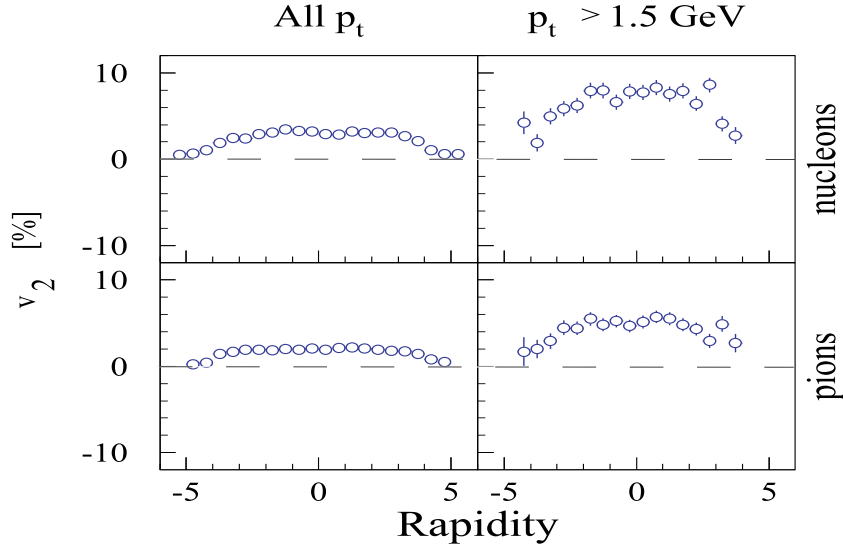


Figure 11. Elliptic-flow coefficient for nucleons and pions from RQMD simulations of $b = (5 - 10)$ fm Au + Au collisions at $\sqrt{s} = 200$ GeV [12].

different EOS, such as in Fig. 2, and different optical potentials

$$U^{opt}(p) = \epsilon(p) - m - T(p), \quad (9)$$

where T is kinetic energy, that either depend or do not on the momentum p in the medium frame.

Typical single-particle observables from the model [13], for different EOS, such as transverse momentum or rapidity distributions, compare favorably to data [14]. Figure 12, with baryon density contour plots from a simulation of the 2 GeV/nucleon Au + Au reaction at $b = 8$ fm, helps to understand the generation of elliptic flow. The simulation was done assuming a hard EOS and a momentum dependence in the baryonic MFs. The participant matter gets compressed in Fig. 12 to $\lesssim 3\rho/\rho_0$ and then explodes when spectator pieces are still present. When the simulation is done in the cascade mode of the model, the participant matter gets compressed to higher densities and it decompresses in quite a sluggish manner. At the completion of the decompression the spectator pieces are far gone. Figure 13 shows next the evolution of the midrapidity elliptic anisotropy in the two simulations. In either of the simulations, the anisotropy begins to grow in the in-plane direction. In the hard-EOS calculation, the growth is rapid and then the anisotropy

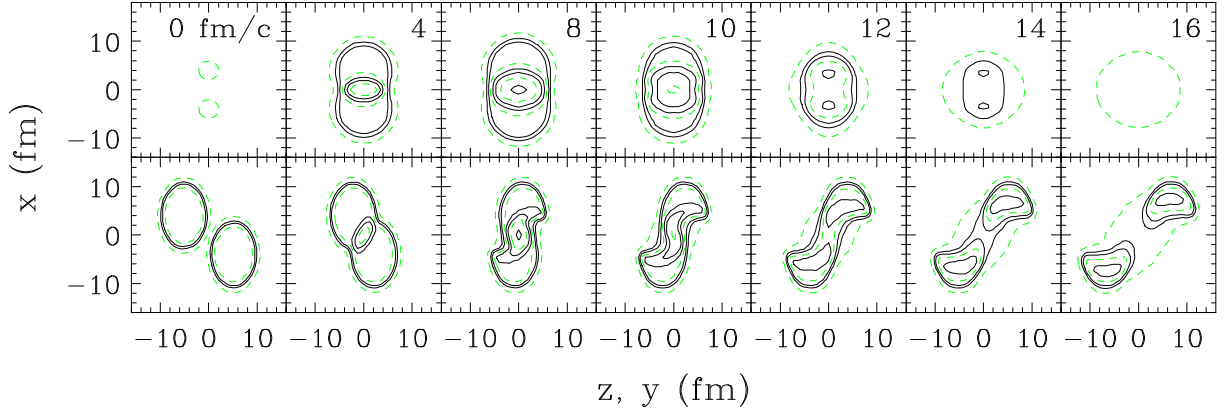


Figure 12. Contour plots of baryon density in the 2 GeV/nucleon Au + Au reaction at $b = 8$ fm in the reaction plane (bottom panels) and in the plane through the system center orthogonal to the beam axis (top panels). The simulation was done assuming a hard EOS and momentum-dependent U^{opt} . The density contours are shown at $\rho/\rho_0 = 0.1, 0.5, 0.8$ and then at 0.4 intervals. Every third contour, i.e. for $\rho/\rho_0 = 0.1, 1.2$, and 2.4 , is represented by a dashed line. The remaining contours are represented by solid lines. Numbers in the figure indicate time in fm/c.

changes its sign. In the cascade calculation the growth is slow and it continues till late times. These findings may be understood as follows. The expansion of the participant region first grows primarily in the in-plane direction as in that direction the pressure gradients are the largest [10]. If the expansion is rapid, though, the matter encounters the spectator pieces on its way. Then the in-plane expansion stalls, while the expansion in the transverse direction can develop. On the other hand, the expansion is slow, the spectator pieces do not present much inhibition and then expansion can continue primarily in the in-plane direction until the complete decompression.

The presence of the spectator pieces allows then to assess the pace of expansion of the participant matter from the elliptic flow for participants. Figure 14 shows the elliptic flow excitation functions for different calculations. The flow turns more in-plane as the beam energy increases and the spectator pieces move faster away from the reaction zone and get shortened by the Lorentz contraction. For the cascade calculation, for which the expansion is sluggish, the flow is of a primarily in-plane character at the displayed energies. The harder the EOS, the more out-of-plane the flow gets. However, there is more sensitivity to the EOS at the low energies when the spectator pieces remain still close to the participant zone than at high. In addition to the EOS, the momentum dependence of MFs felt by the emerging baryons affects their flow. The momentum dependence makes the fields felt by high-momentum particles more repulsive, speeding up the expulsion of these particles from the central participant zone.

Next question is whether a phase transition could sufficiently change the expansion as a function of energy to yield an observable trace in the excitation function for ellipticity. The answer is provided in Fig. 15 that shows the excitation function for a hard EOS with

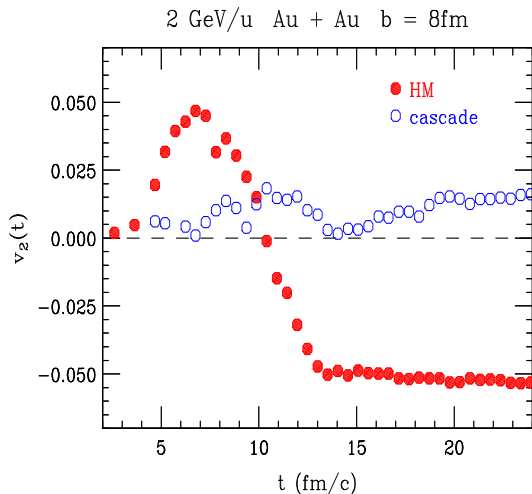


Figure 13. Temporal evolution of the midrapidity elliptic anisotropy in 2 GeV/nucleon Au + Au collision at $b = 8$ fm in the cascade mode of the model (open circles) and for a hard EOS with momentum dependence in the MFs (filled circles).

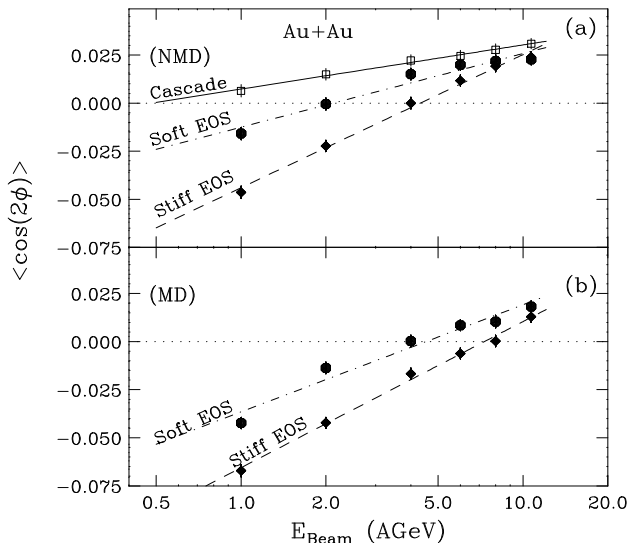


Figure 14. Calculated elliptic flow excitation functions for Au + Au reactions. Panels (a) and (b) show, respectively, the functions obtained without (NMD) and with (MD) the momentum dependent forces. The filled circles, filled diamonds, and open squares indicate, respectively, results obtained using a soft EOS, a stiff EOS, and by neglecting the MF. The straight lines show logarithmic fits.

a phase transition which softens that EOS at higher densities similarly to the case in Fig. 2. At lower energies the excitation function in Fig. 15 follows the hard EOS function, but then it switches to the soft EOS function as the densities reached in the reactions increase.

Now the question is what kind of expansion scenario is followed in Nature. Comparing the data in Fig. 10 to the cascade calculations in Fig. 14 at 1-4 GeV/nucleon, it is apparent that the expansion is much more rapid than in the cascade model at the reached densities. Figure 16 shows next a collection of the data with momentum-dependent calculations superimposed. It is seen that at 2 GeV/nucleon the expansion is as rapid as for the hard EOS with the momentum dependence, represented in Fig. 12. At higher energies, though, the expansion becomes more such as for the soft EOS with behavior as a function of energy strongly reminding that in Fig. 15 for the phase transition.

Below 1 GeV/nucleon different flow data favor a soft EOS with momentum dependence, e.g. [17]. Sideward data favor that EOS in fact up to 10 GeV/nucleon; admittedly, though, the sideward flow is more exposed to the uncertainties in stopping than the elliptic flow. Combining older and the newer higher-energy elliptic and sideward flow results, we can draw broad boundaries for the dependence of pressure on baryon density (or on energy density) as exhibited in Fig. 17. The pressure is certainly higher than in the cascade model;

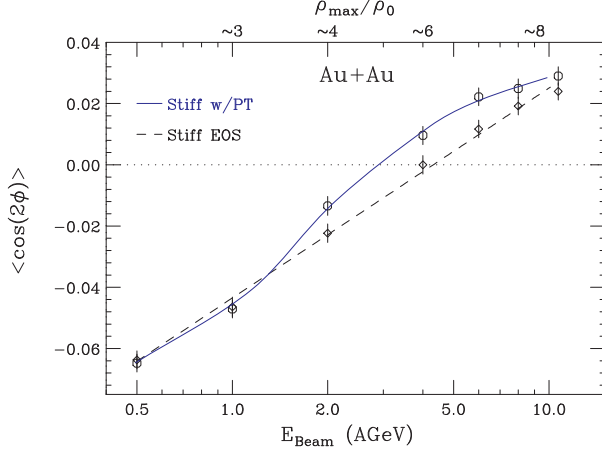


Figure 15. Calculated elliptic flow excitation functions for Au + Au. The diamonds represent results obtained with a stiff EOS. The circles represent results obtained with a stiff EOS and with a second-order phase transition. The lines guide the eye.

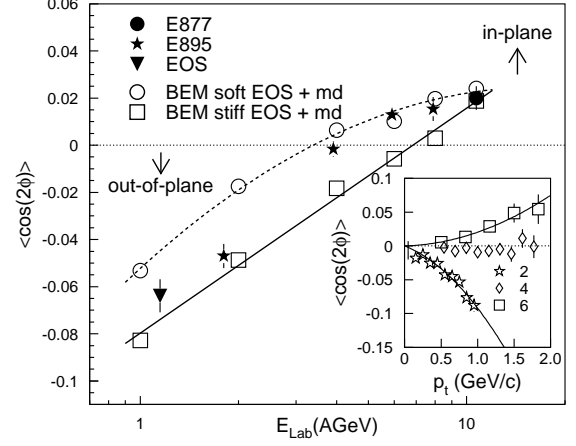


Figure 16. Elliptic-flow excitation function for Au + Au. The data are from Refs. [9], [15], and [16]. Calculations have been carried out for the soft and the stiff EOS with momentum dependence.

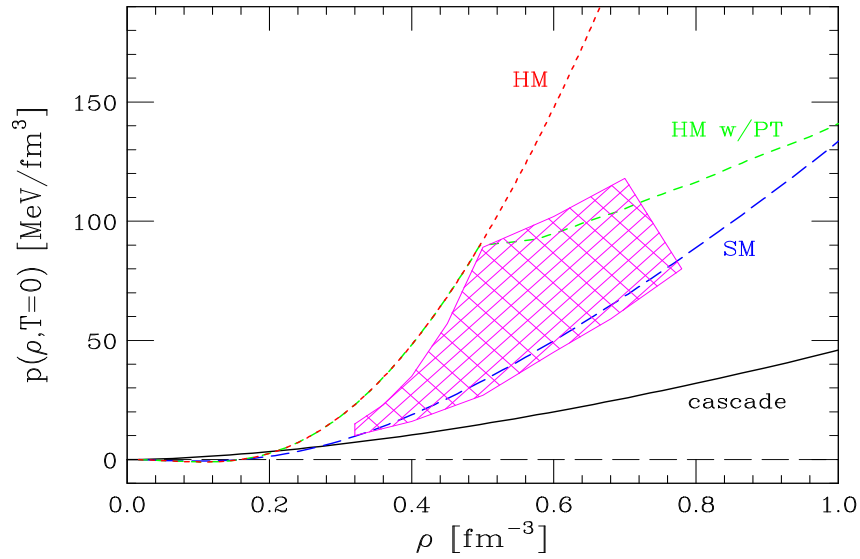


Figure 17. Shaded region shows boundaries on pressure vs baryon density in $T = 0$ symmetric nuclear matter, from flow observables.

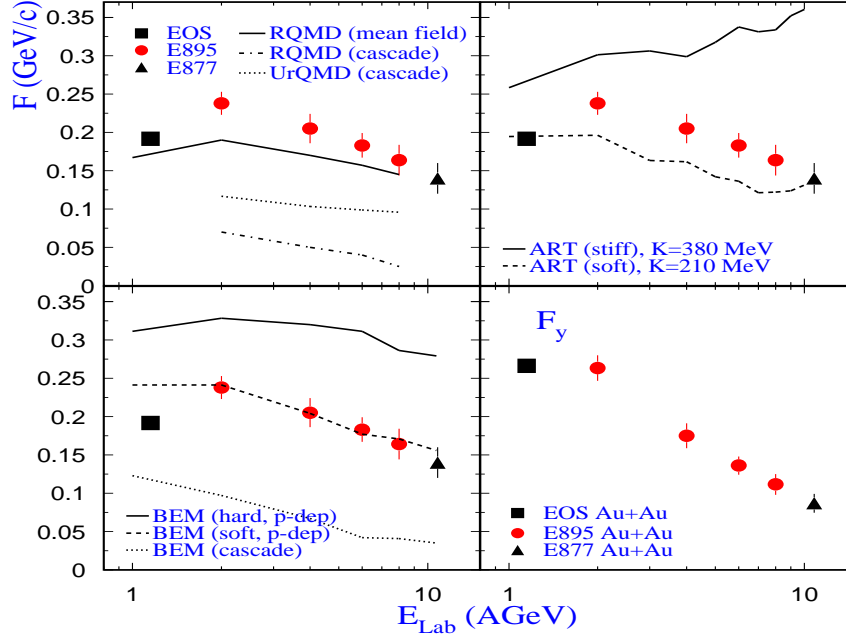


Figure 18. Proton flow magnitude as a function of beam energy; the lower right panel shows the measured F_y , while the other three panels show identical measurements of the parameter F , with different transport model calculations superimposed. The error bars include systematic uncertainties.

other than in the 1-2 GeV/nucleon region (vicinity of the upper boundary kink in Fig. 17) there is no indication of any preference for the hard EOS. A set of sideward flow data with model predictions superimposed is shown in Fig. 18. Contrary to Fig. 16, no evidence for a sudden softening of EOS is seen here. As to conclusions on pressure vs baryon density, those drawn for asymmetric matter from neutron star properties generally pertain [18] to lower densities than in Fig. 17.

Deducing the properties of equilibrium matter requires restricting the range of the dependence of baryonic MFs on momentum. This can be done by examining the dependence of elliptic flow on momentum at the energies of interest.

6. DIFFERENTIAL STUDIES OF FLOW

Studies of flow in narrow intervals of transverse momentum, rapidity and impact parameters can help to disentangle the effects of EOS and other characteristics of strongly interacting matter. Figure 19 shows the dependence of v_2 on impact parameter in Au + Au collisions at 400 MeV/nucleon. At lower impact parameters, the effects of the stiffness of EOS and of mean-field momentum dependence compete with each other. However, at higher impact parameters the predictions for the momentum-independent and momentum-dependent MFs well separate. Additional sensitivity to the momentum dependence might be expected while concentrating on flow at high momenta [17].

Figure 20 compares the ratio of out-of-plane to in-plane proton yields

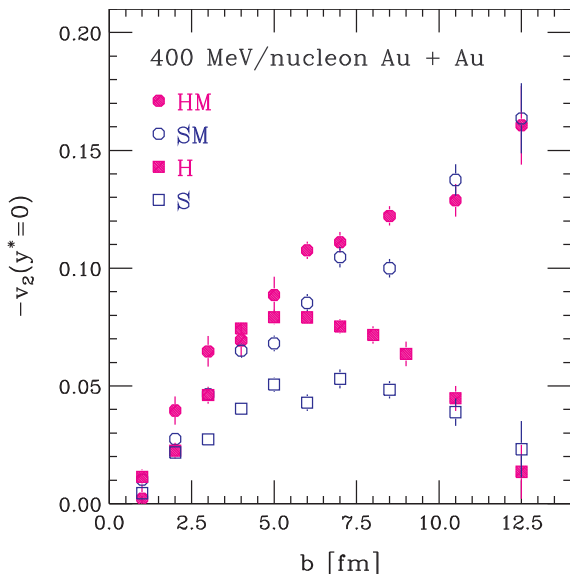


Figure 19. Negative of the ellipticity coefficient at midrapidity, as a function of the impact parameter, from simulations of Au + Au collisions at 400 MeV/nucleon. The squares and circles represent, respectively, the results for MFs without and with momentum dependence. The filled symbols are for the incompressibility $K = 380$ MeV and the open symbols are for $K = 210$ MeV.

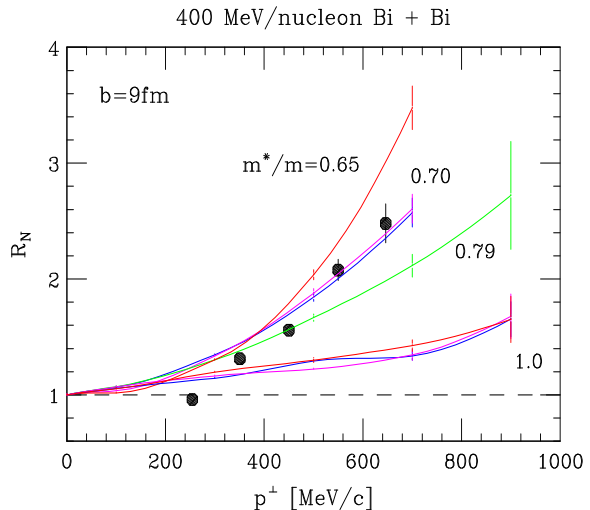


Figure 20. Out-of-plane to in-plane ratio $R_N = (1 - 2v_2)/(1 + 2v_2)$ for protons emitted at midrapidity from 400 MeV/nucleon Bi + Bi reactions, as a function of transverse momentum. Symbols represent data of Ref. [19] while lines represent transport-model calculations for different momentum dependencies in the MF.

$$R_N = \frac{N(90^\circ) + N(270^\circ)}{N(0^\circ) + N(180^\circ)} = \frac{1 - 2v_2}{1 + 2v_2} \quad (10)$$

from KaoS measurements [19] to the results of simulations. It is apparent that the data permit tuning the MF momentum dependence as labeled by the effective mass.

Figure 21 compares next the transport-model parametrizations of MF to the microscopic Dirac-Brueckner-Hartree-Fock (DBHF) calculations with Bonn-A interaction. Within the tested region of densities there is a good agreement between the parametrizations that best describe data [19] and the microscopic calculations. Other microscopic theories exhibit a variable degree of agreement with the optimal parametrizations.

7. CONCLUSIONS

Flow observables are important tools for investigating properties of hadronic matter in energetic collisions. Measurements of second order and first order flow at beam energies $\gtrsim 2$ GeV/nucleon show that the matter is significantly stiffer than in the cascade model. Lower and also upper bounds on the pressure may be deduced as a function of

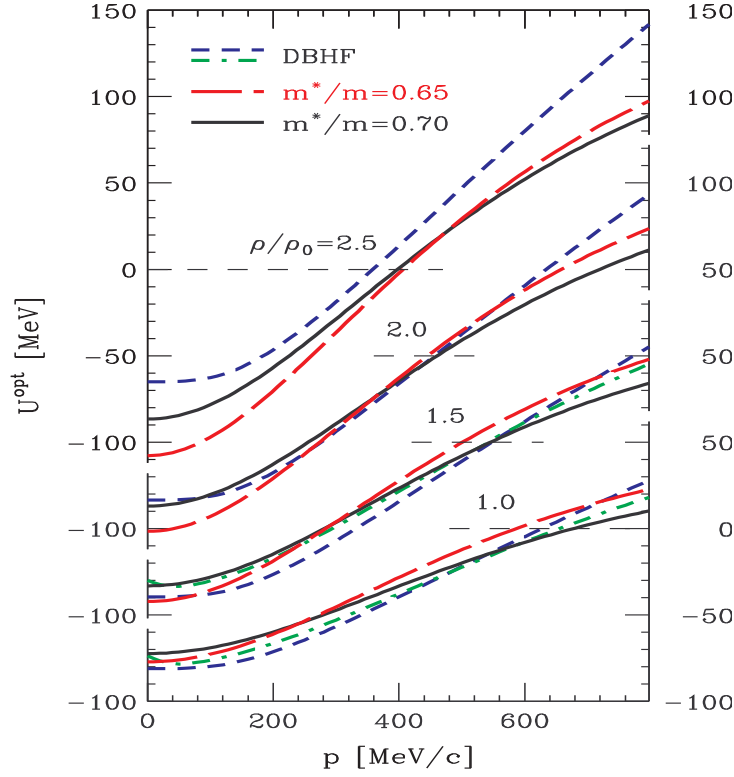


Figure 21. Optical potential in nuclear matter as a function of nucleon momentum, at different densities, from the DBHF calculations with the Bonn-A interaction [20] (short-dashed and short-dash-dotted lines) and in the transport-model parametrizations (solid and long-dashed lines). The thin horizontal dashed lines indicate the zero value for the potential.

density. Dependence of the elliptic flow on momentum probes the dependence of mean field on momentum at supranormal densities and may be used to constrain microscopic theories. Some level of softening may occur in the EOS at the energies between 2 and 4 GeV/nucleon, corresponding to a compression of 3-4 ρ_0 . Further insights could be gained by studying the b -dependence of v_2 .

ACKNOWLEDGEMENT

This work was partially supported by the National Science Foundation under Grant PHY-0070818.

REFERENCES

1. S. Hama *et al.*, Phys. Rev. C 41 (1990) 2737.
2. P. J. Siemens and J. O. Rasmussen, Phys. Rev. Lett. **42**, 880 (1979).
3. G. Poggi *et al.*, Nucl. Phys. **A586** (1995) 755.
4. I. G. Bearden *et al.*, Phys. Rev. Lett. **78** (1997) 2080.

5. P. F. Kolb *et al.*, hep-ph/0006129.
6. J. Barrette *et al.*, Phys. Rev. C 56 (1997) 3254.
7. J. Janicke *et al.*, Nucl. Phys. A536 (1992) 201.
8. P. Danielewicz and Q. Pan, Phys. Rev. C 46 (1992) 2002.
9. C. Pinkenburg *et al.*, Phys. Rev. Lett. 83 (1999) 1295.
10. J.-Y. Ollitrault, Phys. Rev. D 46 (1992) 229.
11. P. Danielewicz and P. V. Ruuskanen, Phys. Rev. D 35 (1987) 344.
12. R. J. M. Snellings *et al.*, nucl-ex/9904003.
13. P. Danielewicz, Nucl. Phys. A661 (1999) 91c.
14. L. Ahle *et al.*, Phys. Rev. C 57 (1998) R466.
15. EOS Collaboration, M. Partlan *et al.*, (unpublished).
16. P. Braun-Munzinger and J. Stachel, Nucl. Phys. A638 (1998) 3c.
17. Q. Pan and P. Danielewicz, Phys. Rev. Lett. 70 (1993) 2062, 3523.
18. J. M. Lattimer and M. Prakash, astro-ph/0002203.
19. D. Brill *et al.*, Zeit. f. Phys. A355, 61 (1996).
20. R. Brockmann and R. Machleit, Phys. Rev. C 42, 1965 (1990).